Eur. J. Mech., A/Solids, 11, n° 2, 215-231, 1992

Cavitation instabilities in a power hardening elastic-plastic solid

V. TVERGAARD *, Y. HUANG ** and J. W. HUTCHINSON **

ABSTRACT. – For an infinite, remotely stressed elastic-plastic solid containing an isolated void a state may be reached, in which the void grows without bound, even though the remote stresses and strains are kept fixed. Such cavitation instabilities are determined here for power hardening elastic-plastic solids subject to axisymmetric stress states. The relatively simple analysis for a spherical void under spherically symmetric conditions is first briefly reviewed. Subsequently, the effect of an axisymmetric stress state is studied for the case of a cylindrical void, where the problem is also governed by ordinary differential equations. For a spherical void under axisymmetric stressing cavitation instabilites are determined by a numerical procedure, which couples a finite element solution for an inner region with a perturbation solution for an outer region. It is found that the critical stress levels are significantly increased by deformation hardening.

1. Introduction

Analyses of void growth in ductile materials usually show that the volumetric growth rate is proportional to the average strain rate in the material and that the growth rate increases strongly with increasing stress triaxiality ([Rice & Tracey, 1969]; [McClintock, 1968]; [Gurson, 1977]; [Budiansky, Hutchinson & Slutsky, 1982]). These analyses are based on the assumption of a rigid-plastic material, but numerical analyses for an elastic-plastic material show the same type of behaviour (e.g. *see* [Tvergaard, 1982]). However, for a cavity in an elastic-plastic material subject to pure hydrostatic tension a critical stress level has been found, at which the void grows without bound for a stationary overall strain ([Bishop, Hill & Mott, 1945]; [Hill, 1950]). The void expansion at this cavitation instability is driven by the elastic energy stored in the surrounding material.

In the context of nonlinear elasticity much interest has recently been devoted to cavitation instabilities ([Ball, 1982]; [Horgan & Abeyaratne, 1986]; [Chou-Wang & Horgan, 1989]). In these investigations the occurrence of a cavitation instability has been interpreted either as a bifurcation from a homogeneously stressed solid to a solid containing a void, or as the growth of a preexisting void. With the exception of recent work by Hou [1990] all the finite elasticity investigations have focussed on the spherically

* Department of Solid Mechanics, The Technical University of Denmark, Lyngby, Denmark.
** Division of Applied Sciences, Harvard University, Cambridge MA 02138, USA.

EUROPEAN JOURNAL OF MECHANICS, A/SOLIDS, VOL. 11, N° 2, 1992
0997-7538/92/02 215 17/$ 3.70/

symmetric problem, or on the analogous problem of a cylindrical void under plane strain axisymmetric conditions.

The occurrence of cavitation instabilities in elastic-plastic materials requires very high stress levels, of the order of 4 or 5 times the yield stress in uniaxial tension, which is not found at a sharp notch or even in front of a blunting crack tip [McMeeking, 1977]. However, very high stress levels due to highly constrained plastic flow are found in ductile reinforcing particles or layers in ceramics, which may lead to cavitation failures such as that observed by Ashby, Blunt & Bannister [1989] in a ductile wire reinforcing a glass matrix. The spherically symmetric stress states, for which cavitation instabilities have been thoroughly investigated, are usually not relevant in such metal-ceramic configurations. Therefore Huang, Hutchinson & Tvergaard [1989] have determined the range of axisymmetric stress states in which cavitation instabilities occur for an elastic-perfectly plastic solid. These axisymmetric cavitation states are characterized by a purely elastic region far from the void, except in a limiting case where the material is fully plastic at cavitation.

In the present paper the investigation of Huang *et al.* [1989] is extended to consider axisymmetric cavitation states for a power hardening elastic-plastic material. The ductile reinforcing wire used in the experiments of Ashby *et al.* [1989] was made of lead, which did show a significant amount of deformation hardening, and the measured peak stresses were significantly above the critical levels corresponding to elastic-perfectly plastic solids. For spherically symmetric conditions the effect of hardening is illustrated by a relatively simple analysis. Axisymmetric cavitation states for the elastic-plastic power hardening material are first studied for a circular cylindrical void, with axis in the principal tensile direction, and subsequently results are shown for a spherical void, using analyses analogous to those employed by Huang *et al.* [1989].

2. Pure hydrostatic tension

For a spherical void in an incompressible elastic-plastic solid under hydrostatic tension spherical symmetries apply, and the analysis given by Huang *et al.* [1989] is relatively simple. A few steps of this analysis are repeated here, to introduce the basic effect of strain hardening on cavitation instabilities.

The uniaxial true stress vs. logarithmic strain relationship is taken to be of the form $\sigma/\sigma_y = f(\varepsilon)$, where σ_y is the initial yield stress. When R_i and R_0 denote the initial and current void radii, respectively, the logarithmic radial and hoop strains of the material element at the current radius R are found by incompressibility as

$$\varepsilon_R = -2\,\varepsilon_\theta = \frac{2}{3}\ln\left[1-(R_0^3-R_i^3)/R^3\right] \tag{2.1}$$

Expressed in terms of the true stress components σ_R and σ_θ in the current configuration at radius R the equation of equilibrium is

$$\frac{d\sigma_R}{dR} + \frac{2}{R}(\sigma_R - \sigma_\theta) = 0 \tag{2.2}$$

with the boundary conditions

$$\sigma_R = 0, \qquad R = R_0 \qquad \text{and} \qquad \sigma_R \to \sigma^\infty \quad \text{as} \quad R \to \infty. \tag{2.3}$$

Integration of (2.2), using (2.3), gives an expression for the remote stress

$$\sigma^\infty = -2\int_{R_0}^{\infty} (\sigma_R - \sigma_\theta)\frac{dR}{R}. \tag{2.4}$$

Due to incompressibility the strains are not affected by superposing a hydrostatic pressure σ_θ on the stress state $(\sigma_R, \sigma_\theta, \sigma_\theta)$, leading to a uniaxial stress $\sigma_R - \sigma_\theta$, and therefore $(\sigma_R - \sigma_\theta)/\sigma_y = f(\varepsilon_R)$. Substituting this into (2.4) and using (2.1) gives the expression

$$\frac{\sigma^\infty}{\sigma_y} = -2\int_1^{\infty} f\left[\frac{2}{3}\ln\left\{1 - \frac{1-(R_i/R_0)^3}{\eta^3}\right\}\right]\frac{d\eta}{\eta}. \tag{2.5}$$

The cavitation limit stress σ_c^∞ is obtained from (2.5) by letting $R_0/R_i \to \infty$

$$\frac{\sigma_c^\infty}{\sigma_y} = -2\int_1^{\infty} f\left[\frac{2}{3}\ln\{1-\eta^{-3}\}\right]\frac{d\eta}{\eta} = -\int_0^{\infty} [e^{(3/2)\xi} - 1]^{-1} f(-\xi)\, d\xi. \tag{2.6}$$

For a power hardening solid the uniaxial stress-strain law is

$$\frac{\sigma}{\sigma_y} = f(\varepsilon) = \begin{cases} \varepsilon/\varepsilon_y, & |\varepsilon| \leqq \varepsilon_y \\ \text{sign}(\varepsilon)\{|\varepsilon|/\varepsilon_y\}^N, & |\varepsilon| > \varepsilon_y \end{cases} \tag{2.7}$$

where $\varepsilon_y = \sigma_y/E$. For this stress-strain behaviour, with $N = 0$, 0.1, 0.2 or 0.3, Figure 1 shows the development of σ^∞/σ_y vs. R_0/R_i, corresponding to $\varepsilon_y = 0.003$. The cavitation instability stresses are approached asymptotically by these curves, and it is seen that the critical stress increases significantly with strain hardening. Values of σ_c^∞ computed by Huang *et al.* [1989] for different values of ε_y show that σ_c^∞ decreases with increasing ε_y.

When the effect of elastic compressibility is accounted for in the analysis for the spherically symmetric problem ([Hill, 1950]; [Huang *et al.* 1989]) the values of σ_c^∞ are slightly reduced. Thus, for Poisson's ratio $\nu = 0.3$ the values found for σ_c^∞ are about 5 pct. lower than those corresponding to the incompressible elastic-plastic solid ($\nu = 0.5$).

It is noted that the instability occurs as a limit point of the remote true stress. Furthermore, when the remote stress state has become constant, at the instability, the remote strains in the infinite solid are also constant. This criterion of instability aplies also to the cases of axisymmetric stressing to be considered in the following.

3. Axisymmetric stressing of cylindrical voids-deformation theory

The choice of multi-axial constitutive law is not at issue in the formulation of the spherically symmetric problem in Section 2 since the deviator stress components increase in exact proportion everywhere within the body. This is not the case for a cylindrical void in an infinite solid under axisymmetric stressing even when the remote stresses are increased proportionally. It has been found that choice of constitutive law (*i.e.* flow versus deformation theory) has a particularly strong influence on the cavitation predictions for the cylindrical void when the remote stresses exceed yield. The cylindrical void problem provides an excellent example to illustrate the distinction between plasticity (flow theory) versus nonlinear elasticity (deformation theory) in so far as cavitation analysis is concerned. Deformation theory results are presented in this section, and flow theory results are presented for the cylindrical void in Section 4.

The material is taken to be incompressible and isotropic. The uniaxial true stress-logarithmic strain relation is written as

$$\sigma/\sigma_y = f(\varepsilon) \tag{3.1}$$

where σ_y is a reference stress which can be identified with an initial yield stress. The J_2 deformation theory is a nonlinear elasticity theory based on the J_2 invariant which generalizes (3.1) to multiaxial stress states [Hutchinson & Neale, 1982]. In the principal axes of stress, the logarithmic strain components are given by

$$\varepsilon_{ij} = f^{-1}\left(\frac{\sigma_e}{\sigma_y}\right)\frac{3\,s_{ij}}{2\,\sigma_e} \tag{3.2}$$

where f^{-1} is the inverse function to f, s_{ij} are the deviator components of the true stress, and $\sigma_e = (3\,s_{ij}\,s_{ij}/2)^{1/2}$ is the effective stress.

An infinitely long, traction-free void with its axis of revolution coincident with the x_3-Cartesian axis is assumed to exist within an infinite solid characterized by (3.2). The solid is subject to remote axisymmetric stressing such that

$$\sigma_{33}^{\infty} = S, \qquad \sigma_{11}^{\infty} = \sigma_{22}^{\infty} = T. \tag{3.3}$$

Let

$$\rho = T/S \tag{3.4}$$

be one measure of remote stress triaxiality, and note that another measure is related by

$$\sigma_m/\sigma_e = (1+2\rho)/[3(1-\rho)] \tag{3.5}$$

for $S > T$ where $\sigma_m = \sigma_{kk}/3$ is the mean stress.

Under the assumption that the deformation is axisymmetric and independent of x_3 (e.g. non-axisymmetric bifurcations are excluded), the expansion of the cylindrical void as a function of S and T can be solved in closed form. The analysis will not be given here. A similar analysis has been carried out by Hou [1990] in the context of a study of

cavitation of cylindrical and spherical voids in nonlinear elastic solids. It is somewhat more involved than the corresponding analysis of the spherically symmetric problem in Section 2. The formula for the values of S and T at the cavitation limit when the void radius becomes unbounded is implicit. With $S > T$ and $T = \rho S$, the value of S at cavitation satisfies

$$\frac{S}{\sigma_y} = \frac{1}{\rho} \int_{\varepsilon}^{\infty} \frac{f(\xi)\, d\xi}{\exp\left[3(\xi^2 - \varepsilon^2)\right]^{1/2} - 1} \tag{3.6}$$

where

$$\varepsilon = \varepsilon_{33}^{\infty} = f^{-1}((1-\rho)\, S/\sigma_y). \tag{3.7}$$

In the limit of remote hydrostatic tension ($\rho = 1$, $\varepsilon = 0$), (3.6) reduces to the result (2.6) for the spherical void, except for a factor $\sqrt{3}$ rather than 3/2 in the argument of the exponential.

Two uniaxial stress-strain curves will be used to illustrate the role of stain hardening on cavitation, the piecewise power law in (2.7) and the Ramberg-Osgood curve

$$\varepsilon/\varepsilon_y = \sigma/\sigma_y + (3/7)(\sigma/\sigma_y)^n \tag{3.8}$$

where, as before, $\varepsilon_y = \sigma_y/E$ and $n = 1/N$. The two curves, (2.7) and (3.8), have the same elastic-perfectly plastic limit as $N \to 0$.

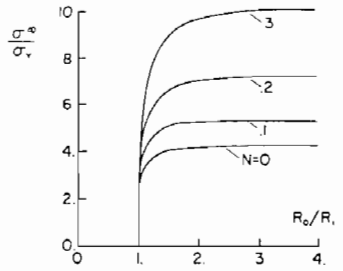

Fig. 1. – Remote stress vs. cavity radius for power hardening incompressible solids ($\nu = 0.5$) with $\sigma_y/E = 0.003$, subjected to spherically symmetric loading.

Cavitation stress states are presented in Figure 2 in the form of S/σ_y and σ_m/σ_y as functions of ρ for two hardening levels, $N = 0.1$ and 0.2, and for $\sigma_y/E = 0.003$. The results are weakly dependent on the details of the stress-strain curve (e.g. piecewise power vs. Ramberg-Osgood), but the primary dependence is on the strain hardening exponent. Trends similar to these are found by Hou [1990]. The cavitation stress states which exceed yield in the remote field lie to the right of the dashed curve labelled $S - T = \sigma_y$. For cavitation states which do not exceed remote yield, the criterion for cavitation is closely approximated by a critical value of σ_m. From (3.6) with $\rho = 1$, this critical value is

$$\sigma_m/\sigma_y = \int_0^{\sigma} \left[e^{\sqrt{3}\,\xi} - 1\right]^{-1} f(\xi)\, d\xi. \tag{3.9}$$

Note that the curve for the elastic-perfectly plastic solid ($N=0$) terminates at $S-T=\sigma_y$ since the effective stress cannot exceed σ_y.

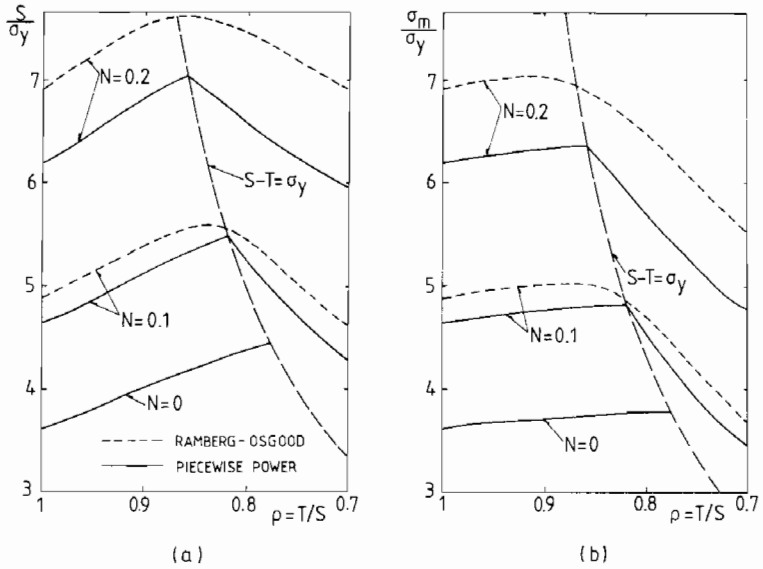

Fig. 2. – Cavitation limits for cylindrical void in deformation theory solid with $\sigma_y/E=0.003$. (*a*) Axial tensile stress; (*b*) Mean stress.

4. Axisymmetric stressing of cylindrical voids-flow theory

The cylindrical cavitation problem is reconsidered for an incompressible solid characterized by the same general form (3.1) for the uniaxial stress-strain curve but generalized to multi-axial stress states by the incremental plasticity relation, J_2 flow theory. In this problem the principal axes of stress and strain of each material element do not rotate. In the principal axes, increments of logarithmic strain components are related to true stress increments for a given material element by

$$\dot{\varepsilon}_{ij}=\frac{3}{2E}\dot{s}_{ij}+\frac{3}{2}\left(\frac{1}{E_t}-\frac{1}{E}\right)\frac{s_{ij}}{\sigma_e}\dot{\sigma}_e \tag{4.1}$$

where s_{ij} and σ_e are defined as before and $E_t\equiv d\sigma/d\varepsilon$ is the slope of the uniaxial true stress-logarithmic strain curve at $\sigma=\sigma_e$. The second term in (4.1) is taken to be zero when σ_e is below yield or if elastic unloading occurs.

The flow theory version of the problem is intrinsically incremental. However, the incremental equations can be reduced significantly such that generation of numerical results requies only numerical integration and an associated updating of the stress distribution.

The problem is one of generalized plane strain. Let ε denote the logarithmic strain in the x_3 direction, parallel to the axis of the cylindrical void, with $\dot{\varepsilon}$ as its increment.

Incompressibility and axial symmetry result in nonzero velocity and strain components which are given by (in cylindrical components)

$$v_R = -\frac{1}{2}\dot{\varepsilon} R + \dot{A} R^{-1}, \qquad v_3 = \dot{\varepsilon} x_3 \tag{4.2}$$

$$\dot{\varepsilon}_R = -\frac{1}{2}\dot{\varepsilon} - \dot{A} R^{-2}, \qquad \dot{\varepsilon}_\theta = -\frac{1}{2}\dot{\varepsilon} + \dot{A} R^{-2} \tag{4.3}$$

where $\dot{A}$ is a free amplitude and R is the distance to the material element from the central axis in the current configuration.

The incremental equation of equilibrium written in the current configuration can be reduced with the aid of the constitutive law and the traction-free condition on the void surface to the following equation relating $\dot{A}$ and $\dot{\varepsilon}$

$$\dot{A}\left\{\frac{2}{3} E R_0^{-2} - \int_{R_0}^{\infty} (E - E_t)(s_R - s_\theta)^2 \sigma_e^{-2} R^{-3}\, dR + 2\int_{R_0}^{\infty} (s_R - s_\theta) R^{-3}\, dR\right\} = \dot{\varepsilon}\left\{\rho(1-\rho)^{-1} E_t^{\infty} + \frac{3}{2}\int_{R_0}^{\infty} (E - E_t)(s_R^2 - s_\theta^2)\sigma_e^{-2} R^{-1}\, dR\right\} \tag{4.4}$$

where R_0 is the current radius of the void. The stresses and tangent modulus in (4.4) are the current values which are functions of R. Where yield has not yet occured or where elastic unloading has occured, $E_t \equiv E$. The above equation was derived under the assumption that the remote stresses are increased proportionally with $\dot{T} = \rho \dot{S}$ with ρ fixed; E_t^{∞} denotes the tangent modulus evaluated at S − T, which is E if S − T is below yield. The equations for updating the stresses in a material element currently located a distance R from the axis are

$$\begin{cases} \dot{s}_R = \left[-\frac{1}{3} E - \frac{3}{2}(E - E_t) s_R s_3 \sigma_e^{-2}\right]\dot{\varepsilon} + \left[-\frac{2}{3} E + (E - E_t) s_R (s_R - s_\theta)\sigma_e^{-2}\right]\dot{A} R^{-2} \\ \dot{s}_\theta = \left[-\frac{1}{3} E - \frac{3}{2}(E - E_t) s_\theta s_3 \sigma_e^{-2}\right]\dot{\varepsilon} + \left[\frac{2}{3} E + (E - E_t) s_\theta (s_R - s_\theta)\sigma_e^{-2}\right]\dot{A} R^{-2} \end{cases} \tag{4.5}$$

with $\dot{s}_3 = -\dot{s}_R - \dot{s}_\theta$.

The results presented below were obtained by numerically integrating the above system of equations. The process is started at an applied stress level at which the entire solid is within the elastic range with a known elastic solution. With V_0 as the initial volume of the void (say, a segment with unit initial length and radius r_0), the current volume of the same void segment is

$$V/V_0 = (R_0/r_0)^2 e^{\varepsilon}. \tag{4.6}$$

A material element initially a distance r from the axis lies a distance R from the axis in the current configuration where

$$R/R_0 = \{(V_0/V)[(r/r_0)^2 - 1] + 1\}^{1/2}. \tag{4.7}$$

Cavitation states for J_2 flow theory with the piecewise power stress-strain curve (2.7) are plotted in Figure 3. When the remote stress state is within the elastic range (e.g. to the left of the line $S-T=\sigma_y$ in the figure), the cavitation instability is unambiguous. Such a state is determined by the condition that $\dot{V}/(\dot{\varepsilon}V)$ is unbounded as the state is approached from below; these states are represented by the solid line curves in Figure 3. For states which correspond to remote yielding, to the right of the curve on which $S-T=\sigma_y$, the cavitation instability criterion was not attained even for volume expansions as large as $V/V_0=500$. Dashed-line curves showing the stress states at which three levels of volume expansion are attained are included in Figure 3.

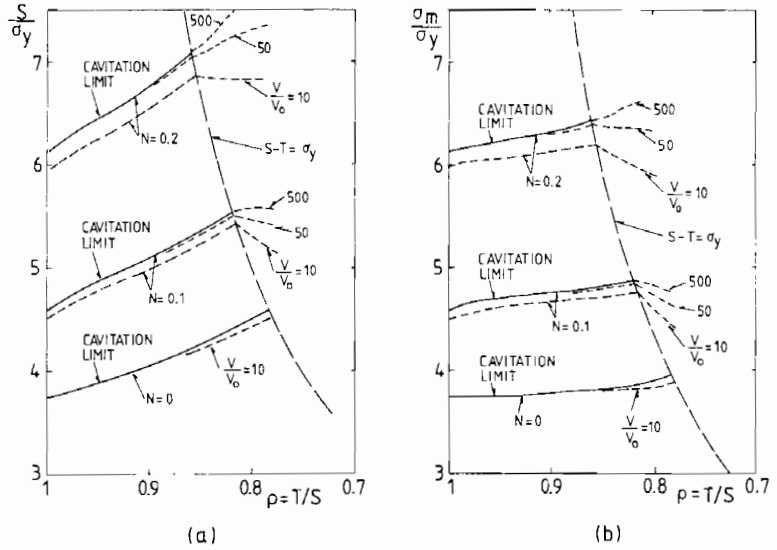

Fig. 3. – Cavitation limits and curves of specified void growth for cylindrical void in flow theory solid with piecewise power law and $\sigma_y/E=0.003$. (*a*) Axial tensile stress; (*b*) Mean stress.

Further insight into the transition in behaviour associated with remote plastic yielding is gained from Figure 4 which displays a normalized dilatation rate as a function of V/V_0 for various levels of triaxiality on either side of the transition. The example shown is for $\sigma_y/E=0.003$ and $N=0.1$ for which $\rho=0.82$ is the smallest value such that cavitation occurs without remote plastic yielding. The measure of dilatation, $\dot{V}/(\dot{\varepsilon}V)$, is normalized by its value at $V/V_0=2$. The curves in Figure 4 reveal a sharp transition in behaviour at $\rho=0.82$. The analysis was not carried to values of V/V_0 larger than 500, and thus at is not possible to rule out the possibility of cavitation at even larger values when $\rho\leqq 0.81$.

Comparison of Figures 2 and 3 reveals that the deformation theory predictions for the cavitation limit are only very slightly lower than those for flow theory when cavitation takes place without yielding in the remote field. Thus, (3.6) is approximately applicable to J_2 flow theory as long as remote yielding does not occur.

A difference in behaviour between the deformation theory and flow theory when remote yielding occurs is not entirely surprising since, then, the stress history of a material element becomes highly non-proportional. Figure 5 shows the yield surface on a (s_R, s_3)

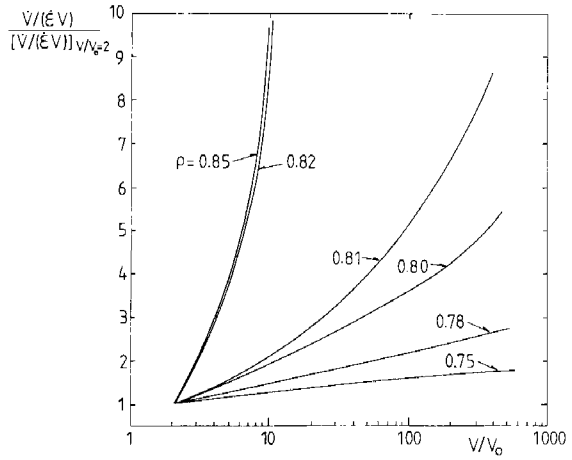

Fig. 4. – Normalized dilatation rate vs. void volume for cylindrical void in flow theory solid with $\sigma_y/E = 0.003$ and $N = 0.1$ (piecewise power law).

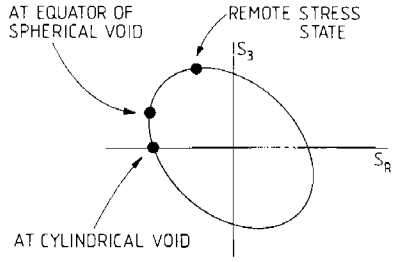

Fig. 5. – Stress states at various material points indicated on yield surface.

trace of deviator stress space ($s_0 = -s_R - s_Z$), for the limit of no hardening. The states associated with remote yielding and with material elements at the surface of the void at cavitation are indicated. Thus, material elements initially far from the void surface must pass from one stress state to the other as they are engulfed by the expanding void in the cavitation process. The change in stress state involved in the cavitation of a spherical cavity is somewhat less than for the cylindrical cavity.

To conclude this section results are presented in Figure 6 for the normalized dilatation rate of the cylindrical void in the elastic-perfectly plastic ($N = 0$) flow theory solid. The range of σ_m/σ_y shown is such that remote yielding occurs and thus $\dot{\varepsilon} \equiv \dot{\varepsilon}^{\infty}_{33}$ is the remote plastic strain rate. The rigid-perfectly plastic result ($\sigma_y/E = 0$, $N = 0$) of McClintock (1968),

$$[\dot{V}/(\dot{\varepsilon}V)]_0 = \sqrt{3}\sinh\left[\sqrt{3}\,\rho/(1-\rho)\right] \tag{4.8}$$

is used for scaling. The values of $\dot{V}/(\dot{\varepsilon}V)$ are those when $V/V_0 \cong 10$, but the values are essentially independent of V/V_0. The trend with σ_y/E shown in Figure 6 is the same as that found for spherical voids by Huang, *et al.* (1990). For a given σ_y/E, the dilatation rate becomes unbounded as σ_m/σ_y approaches from below the value of triaxiality associated with cavitation. In the limit of a rigid-perfectly plastic solid ($\sigma_y/E \to 0$), no cavitation instability occurs.

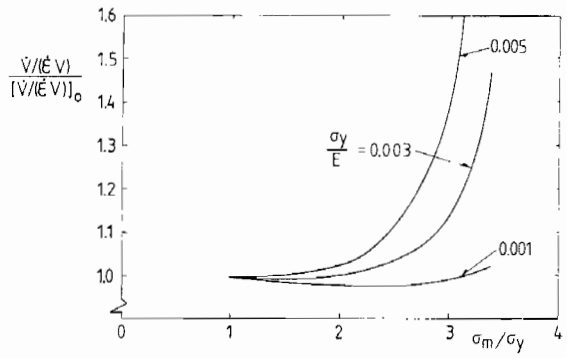

Fig. 6. – Normalized dilatation rate vs. mean stress for cylindrical void in elastic-perfectly plastic flow theory solid (N = 0).

5. Axisymmetric cavitation states for a spherical void

The method used by Huang *et al.* [1989] to analyse cavitation instabilities for an isolated spherical void in an infinite, remotely stressed elastic-perfectly plastic solid is here extended to a power-law hardening solid. The remote stresses, leading to an axisymmetric stress-state, are taken to be

$$\sigma^{\infty}_{33} = S, \qquad \sigma^{\infty}_{11} = \sigma^{\infty}_{22} = T \tag{5.1}$$

where $S \geqq T$. With the material characterized by isotropic hardening J_2 flow theory, plastic yielding in a material point starts when the effective Mises stress σ_e equals the initial yield stress σ_y. Thus, the remote field remains elastic when $S - T < \sigma_y$, whereas yielding occurs remotely when $S - T \geqq \sigma_y$.

5.1. Method of analysis

The numerical analysis for this cavitation problem is based on a Lagrangian formulation of the field equations, using a cylindrical reference coordinate system, in which $x^1 (= r)$, $x^2 (= \theta)$ and $x^3 (= z)$ are the radial, circumferential and axial coordinates, respectively. In terms of the displacement components u^i on the reference base vectors, and the covariant derivatives $u^i_{,j}$ in the reference frame, the Lagrangian strains are given by

$$\eta_{ij} = \frac{1}{2}\,(u_{i,j} + u_{j,i} + u^k_{,i}\, u_{k,j}) \tag{5.2}$$

The contravariant components of the Kirchhoff stress tensor τ^{ij} and the Cauchy stress tensor σ^{ij} are related by

$$\tau^{ij} = \sqrt{G/g}\,\sigma^{ij} \tag{5.3}$$

where g and G are the determinants of the metric tensors g_{ij} and G_{ij} in the reference configuration and the current configuration, respectively. The equilibrium equations are

expressed in terms of the principle of virtual work

$$\int_V \tau^{ij}\,\delta\eta_{ij}\,dV = \int_A T^i\,\delta u_i\,dA \tag{5.4}$$

where V and A are the reference volume and surface, respectively, and T^i are the nominal traction components.

The elastic-plastic material behaviour is represented by a finite strain generalization of J_2 flow theory [Hutchinson, 1973]. The multiaxial incremental stress-strain relationship is of the form $\dot{\tau}^{ij} = L^{ijkl}\,\dot{\eta}_{kl}$, with the tensor of instantaneous moduli given by

$$L^{ijkl} = \frac{E}{1+\nu}\left\{\frac{1}{2}\,(G^{ik}G^{jl}+G^{il}G^{jk}) + \frac{\nu}{1-2\nu}\,G^{ij}G^{kl} - \beta\,\frac{3}{2}\,\frac{E/E_t - 1}{E/E_t - (1-2\nu)/3}\,\frac{s^{ij}s^{kl}}{\sigma_e^2}\right\} - \frac{1}{2}\,(G^{ik}\tau^{jl}+G^{jk}\tau^{il}+G^{il}\tau^{jk}+G^{jl}\tau^{ik}) \tag{5.5}$$

Here, E is Young's modulus, ν is Poisson's ratio, $s^{ij} = \tau^{ij} - G^{ij}\tau^k_k/3$ are the components of the Kirchhoff stress deviator, and $\sigma_e = (3\,s_{ij}s^{ij}/2)^{1/2}$ is the corresponding effective Mises stress. The tangent modulus E_t is the slope of the uniaxial stress-strain curve (2.7), and the value of β is 1 or 0 for plastic yielding or elastic unloading, respectively.

The finite strain generalization of J_2 flow theory employed here is formulated directly in terms of Kirchhoff stresses rather than Cauchy stresses [*see* Hutchinson, 1973], and thus the value of the effective Mises stress σ_e used in (5.5) is $\sqrt{G/g}$ times the corresponding effective stress value defined in terms of Cauchy stresses. Therefore, the condition for the onset of remote yielding is actually $\sqrt{G/g}\,(S-T) = \sigma_y$ in the present computations, rather than $S - T = \sigma_y$. This difference is small, since G/g differs from unity only due to elastic compressibility.

The solution procedure couples an outer solution to a finite element representation of the solution in an inner region. The void considered is initially spherical with radius R_i, and a concentric spherical surface with initial radius R^* is chosen to separate the inner and outer regions. When the remote stress state is in the elastic range, $S - T < \sigma_y$ and R^* is chosen large enough so that the inner region contains all the yielded material surrounding the void, the outer solution is purely elastic. This elastic outer solution has been specified by Huang *et al.* [1989] and shall not be repeated here.

When the remote stress state is in the plastic range, $S - T \geqq \sigma_y$, the outer solution must account for plastic deformations. This solution is approximated by a perturbation analysis analogous to that described in some detail by Huang *et al.* [1989] for the case of perfect plasticity. The solution consists of the uniform field corresponding to a uniform stress state equal to the remote stresses, with the lowest order perturbation superposed. This lowest order perturbation decays to zero as $R \to \infty$. In terms of the spherical coordinates R and θ in the current configuration the displacement increments are

$$\begin{cases} \dot{u}_r = \dot{\varepsilon}^\infty_r\,R\sin\theta - B_0\,R^{-2}\,\dot{u}^B_r(\theta) - C_0\,R^{-2}\,\dot{u}^C_r(\theta) \\ \dot{u}_z = \dot{\varepsilon}^\infty_z\,R\cos\theta - B_0\,R^{-2}\,\dot{u}^B_z(\theta) - C_0\,R^{-2}\,\dot{u}^C_z(\theta) \end{cases} \tag{5.6}$$

and the nominal traction rates on the spherical surface with radius $R = R^*$ have the form

$$(5.7)\qquad \begin{cases} \dot{T}_r = [(C_{11} + C_{12} - T)\dot{\varepsilon}_r^{\infty} + C_{13}\dot{\varepsilon}_z^{\infty}]\sin\theta \\ \quad + B_0 R^{-3}\dot{T}_r^{B}(\theta) + C_0 R^{-3}\dot{T}_r^{C}(\theta) \\ \dot{T}_z = [2C_{13}\dot{\varepsilon}_r^{\infty} + (C_{33} - S)\dot{\varepsilon}_z^{\infty}]\cos\theta \\ \quad + B_0 R^{-3}\dot{T}_z^{B}(\theta) + C_0 R^{-3}\dot{T}_z^{C}(\theta) \end{cases}$$

Here, $\dot{\varepsilon}_r^{\infty}$ and $\dot{\varepsilon}_z^{\infty}$ are the remote true strain rates, and C_{11}, C_{12}, C_{13} and C_{33} are instantaneous moduli corresponding to the uniform field. The perturbations are represented by $\dot{u}_r^B$, $\dot{u}_r^C$, $\dot{u}_z^B$, $\dot{u}_z^C$, $\dot{T}_r^B$, $\dot{T}_r^C$, $\dot{T}_z^B$ and $\dot{T}_z^C$, which are functions of θ, ant the constants B_0 and C_0 are to be determined in the analysis.

Clearly, the elastic outer solution cannot be used near the void, where plastic yielding occurs. But also the plastic outer solution is limited to regions far from the void, in which the lowest order perturbation is still sufficient to give a reasonable approximation of the actual elastic-plastic deformations.

Coupling of the inner and outer solutions requires continuity of displacement increments and nominal traction increments across the spherical surface with radius $R = R^*$. Geometrical compatibility with the outer solution is enforced by using a Lagrange multiplier method (*see* also [Huang *et al.*, 1989]). Thus, in the incremental form of the principle of virtual work (5.4)

$$(5.8)\qquad \int_V \{\dot{\tau}^{ij}\delta\eta_{ij} + \tau^{ij}\dot{u}^k_{,i}\,\delta u_{k,j}\}\,dV - \int_A \dot{T}^i\,\delta u_i\,dA - \int_A \delta\lambda_r[\dot{u}_1 - \dot{u}_r^0]\,dA - \int_A \delta\lambda_z[\dot{u}_3 - \dot{u}_z^0]\,dA = 0$$

the last two surface integrals are added, in which the displacement increments $\dot{u}_i$ on the outside of the inner spherical region are represented by the finite element approximation for the inner region, while $\dot{u}_r^0$ and $\dot{u}_z^0$ are the corresponding functions for the outer solution, given by (5.6) in the case of plastic outer field. The expressions for $\dot{T}^i$ obtained from the outer solution are substituted in the second term of (5.8).

A convenient choice for the variations of the Lagrangian multipliers is

$$(5.9)\qquad \delta\lambda_r = \delta B_0 R^{-3}\dot{T}_r^B(\theta) + \delta C_0 R^{-3}\dot{T}_r^C(\theta)$$

$$(5.10)\qquad \delta\lambda_z = \delta B_0 R^{-3}\dot{T}_z^B(\theta) + \delta C_0 R^{-3}\dot{T}_z^C(\theta)$$

which is also substituted into (5.8). Then, using a finite element approximation with N nodal degrees of freedom in the inner region, the variational equation (5.8) gives $N+2$ linear algebraic equations, where the last two unknowns are the integration constants B_0 and C_0 in the outer solution.

Due to symmetry about the mid-plane $z = 0$ only half of the inner spherical region needs to be analysed numerically. Quadrilateral axisymmetric elements are used, each built up of four triangular linear displacement elements. All solutions are started from a uniform stress state equal to that initially specified at infinity. The initial loads applied to the spherical void surface in order to obtain the uniform stress state are subsequently stepped down over a number of increments until the void surface is free of tractions. During the incremental solution standard equilibrium correction terms are applied at all

nodal points inside the outer surface to avoid drifting away from the true equilibrium path (e. g. *see* [Tvergaard, 1990]).

5.2. Numerical results

The analyses for elastic outer fields are carried out such that the stresses at infinity, S and T, are kept fixed, with $\dot{\varepsilon}_z^\infty = \dot{\varepsilon}_r^\infty = 0$ throughout the computation, while the void growth is precribed. The loads on the void surface are taken to be proportional with a load parameter λ, which has the initial value $\lambda = 1$ corresponding to the initial uniform stress state. In the linear algebraic equations the right hand side proportional to $\dot{\lambda}$ is exchanged with a column corresponding to a radial nodal displacement increment on the void surface, and thus $\dot{\lambda}$ is calculated for a prescribed increment of the chosen nodal displacement. In this manner the development of the load parameter λ is calculated incrementally as a function of the void volume V. If λ becomes negative, the remote stresses are below the cavitation limit, whereas if λ remains postive, the remote stresses exceed the cavitation limit.

This procedure, in which loads on the void surface are stepped down from an initial level corresponding to the fixed remote stresses, will give a stress history in the material near the void that differs from that corresponding to a stress-free void surface. However,

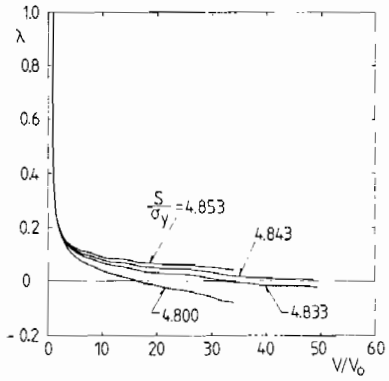

Fig. 7. — Surface load parameter λ vs. void volume V for spherical void, where $\rho = T/S = 0.95$, $\sigma_y/E = 0.003$, $\nu = 0.3$ and $N = 0.05$. Remote strain and stress states are kept fixed.

as is seen in Figure 7, most of the surface load is removed while the void growth is small, and it is expected that the slightly different stress history has little effect on the predicted stress level at the cavitation instability.

Figure 7 shows an example of λ vs. V curves calculated by the procedure described above, for a material characterized by the parameters $\sigma_y/E = 0.003$, $\nu = 0.3$ and $N = 0.05$, and for $\rho = 0.95$. From these curves the cavitation limit is estimated as $S/\sigma_y \simeq 4.84$. It is noted that the curves oscillate due to the finite element approximation of the plastic fields spreading around the void. Similar curves for some other cases have shown stronger oscillations, even with the λ-value varying between positive and negative values, so that the average λ-value has been used to estimate the cavitation limit.

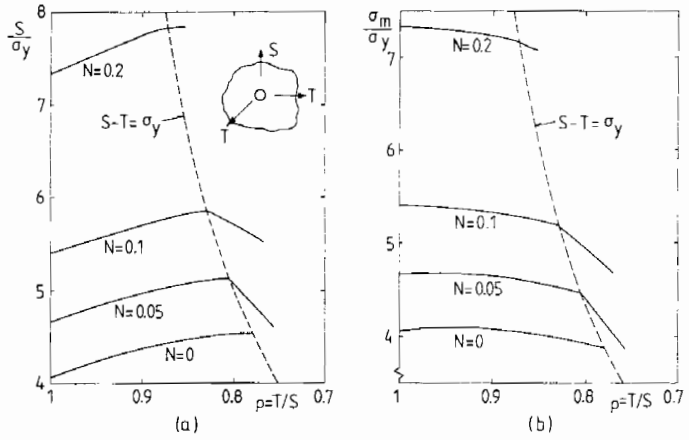

Fig. 8. – Cavitation limits for a spherical void in elastic-plastic power hardening solid subject to remote axisymmetric stressing ($\sigma_y/E=0.003$ and $\nu=0.3$). (*a*) Axial tensile stress; (*b*) Mean stress.

In Figure 8*a* the solid curves show the dependence of the cavitation limit S/σ_y on the remote stress ratio $\rho=T/S$. The material parameters are $\sigma_y/E=0.003$ and $\nu=0.3$, and results are shown for $N=0$ (elastic-perfectly plastic solid). $N=0.05$, $N=0.1$ and $N=0.2$. In the range of elastic remote stress states, $S-T<\sigma_y$, these curves have been determined by a large number of computations as those illustrated in Figure 7. The computations in Figure 7 are stopped at $V/V_0\simeq 50$, but in some cases the computations have been continued until V/V_0 exceeds 1000. In most cases an inner region specified by $R^*/R_i=100$ is sufficiently large to include the maximum extent of the plastic region, but a larger value, $R^*/R_i=1000$, has been needed in a few cases.

For spherically symmetric conditions ($\rho=1$) the critical values of S/σ_y found in Figure 8*a* are slightly lower than those found in Figure 1 (of the order of 5 pct.), because elastic compressibility is accounted for in Figure 8*a*. When the value of the stress ratio ρ decreases, the critical values of S increase a little, following the trends already found by Huang *et al.* [1989] for elastic-perfectly plastic solids in the range where the remote fields are elastic. Also the value of the remote mean stress, $\sigma_m=S(1+2\rho)/3$, at a cavitation instability is of interest, and Figure 8*b* shows critical values of σ_m/σ_y vs. ρ.

The behaviour after the onset of remote yielding (dashed curve in *Fig.* 8) differs significantly from that found by Huang *et al.* [1989]. For an elastic-perfectly plastic solid a cavitation instability with remote plastic yielding occurs only at one value of ρ, corresponding to the intersection of the dashed curve and the solid curve for $N=0$ in Figure 8. However, for a strain hardening material cavitation instabilities with remote plastic yielding may be found in a range of ρ-values. For an elastic-perfectly plastic solid the remote stresses cannot exceed the values on the dashed curve in Figure 8; but this is possible in the presence of strain hardening, and the solid curves in the range $S-T>\sigma_y$ of Figure 8 indicate that a cavitation instability may be reached after a finite amount of plastic straining in the remote fields.

The cavity growth under remote plastic yielding has been analyseed by a direct incremental procedure, in which an increasing remote strain ε_z^∞ is prescribed, while the

stress ratio ρ is kept fixed. Here, the initial uniform stress state is chosen corresponding to the point on the dashed curve ($S-T=\sigma_y$), so that the plastic outer solution (5.6)-(5.7) can be used throughout the analysis. When the initial loads applied to the void surface are stepped down to zero, elastic unloading occurs in rather large regions of material near the poles of the void, and ε_z^* is simultaneously increased to avoid unloading near the interface with the outer solution. Subsequently, this unloaded region becomes smaller, but part of it remains throughout the computation. The direct incremental procedure applied here is quite unstable when the dilatation rate or the void volume grow large. Furthermore, it turns out that the predictions show some sensitivity to the size of the inner region, which indicates that for the strain hardening material the lowest order perturbation solution in the outer region is only accurate for small deviations from the uniform stress state. Thus, in the case of $N=0.1$ and $\rho=0,81$ the values of the critical stresses predicted are $S/\sigma_y \simeq 5.54$ for $R^*/R_i=31.6$, $S/\sigma_y \simeq 5.71$ for $R^*/R_i=100$, $S/\sigma_y \simeq 5.77$ for $R^*/R_i=316$, and $S/\sigma_y \simeq 5.77$ for $R^*/R_i=1000$. It appears that the predicted instability limit has converged for $R^*/R_i=316$, and this value has been used to plot the curves in Figure 8.

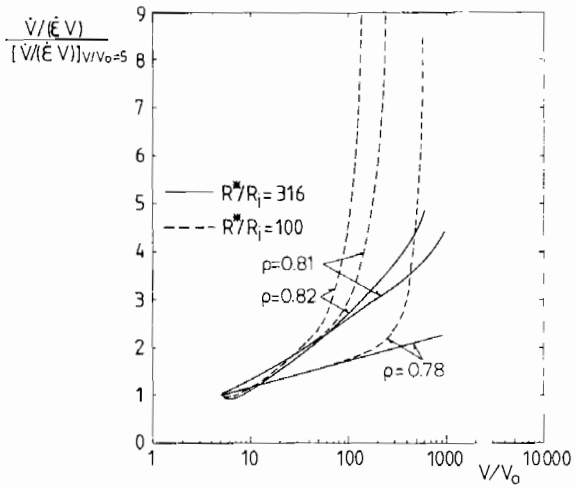

Fig. 9. – Normalized dilatation rate vs. void volume for spherical void in flow theory solid with $\sigma_y/E=0.003$ and $N=0.1$.

Normalized dilatation rates as functions of V/V_0 are shown in Figure 9 for $N=0.1$ and $\sigma_y/E=0.003$. Here, the predictions for $R^*/R_i=100$ show that the dilatation rates grow very large at essentially constant values of V/V_0, thus indicating the existence of a cavitation instability. However, for a larger inner region, $R^*/R_i=316$, the dilatation rates grow less rapidly, and the solid curves in Figure 9 are stopped due to numerical instabilities that occur at $V/V_0 \simeq 1000$, when the strains near the void surface are very large. With the approximations used the predictions for the larger inner region are the more accurate and therefore, as in Figure 4, the results do not prove that a strict cavitation state is reached for the spherical void under remote yielding. But the solid curves predicted in the remote yielding range of Figure 8, for different values of R^*/R_i, are very close with essentially the same slope. Therefore, the results in Figure 8 are more like the results of Figure 2 (deformation theory solid) than those of Figure 3, which

indicates that the spherical voids under remote yielding may actually show a cavitation instability.

The solid curve for $N=0.2$ with plastic remote fields in Figure 8 is nearly horizontal. For $N=0.1$ the corresponding curve decays with decreasing ρ, and the curve for $N=0.5$ decays even more, approaching the slope of the dashed curve. It is noted that these curves show only the initial trends, since no attempt has been made here to determine limiting values of ρ below which there is no indication of a cavitation instability for given material parameters. We do know, however, that in the limit $N \to 0$ the curves for $S-T \geqq \sigma_y$ shrink to a point.

It is seen (in *Fig. 8 b*) that the values of the stress triaxiality parameter σ_m/σ_e needed to reach cavitation instabilities are indeed very high. However, such high stress triaxialities are of practical importance in ductile reinforcing particles or layers in ceramics. Here, the lack of plasticity in the ceramics gives rise to highly constrained plastic flow in the ductile material, as long as the bonding remains intact on the metal/ceramic interface.

The experimental investigations of Ashby *et al.* [1989] for a ductile wire reinforcing a glass matrix were carried out for lead wires, which showed rather strong deformation hardening corresponding to $N \simeq 0.25$. In several cases the fracture surface contained one dimple, showing that a single void had grown until it occupied almost one half of the cross-section of the wire, as might be expected if a cavitation instability had been reached. The peak values of S/σ_y observed in these experiments were in several cases around 6 or even 7, which appears to be in fairly good agreement with the results shown in Figure 8 *a*. It is noted that the axisymmetric stress state in the ductile wire during failure must differ significantly from spherical symmetry, since transverse straining is essentially prevented by the glass matrix.

For the purpose of predicting cavitation stress states, two observations are useful. The shape of the nucleating void does not seem to have a very strong influence on the cavitation state as evidenced by the relatively little difference between the results for spherical and cylindrical voids. In each instance, a critical value of the mean stress serves as a reasonable criterion for characterizing the cavitation state. That critical value depends on the uniaxial stress-strain curve of the material and can be determined using the spherically symmetric result (2.6) or the slightly more conservative result for the cylindrical geometry (3.9).

Acknowledgement

The work of YH and JWH was supported in part by grants NSF-DMR-89-20490 and NSF-MSM-88-12779 and in part by the Division of Applied Sciences, Harvard University.

REFERENCES

ASHBY M. F., BLUNT F. J., BANNISTER M., 1989, Flow characteristics of highly constrained metal wires, *Acta Metallurgica*, **37**, 1857.

BALL J. M., 1982, Discontinuous equilibrium solutions and cavitation in nonlinear elasticity, *Phil. Trans. R. Soc. London*, **A 306**, 557-610.

BISHOP R. F., HILL R., MOTT N. F., 1945, The theory of indentation and hardness tests, *Proc. Phys. Soc.*, **57**, 147-159.

BUDIANSKY B., HUTCHINSON J. W., SLUTSKY S., 1982, *Void growth and collapse in viscous solids* Mechanics of solids, The Rodney Hill 60th Anniversary Volume, H. G. HOPKINS, M. J. SEWELL Eds., Pergamon Press, 13-45.

CHOU-WANG M.-S., HORGAN C. O., 1989, Void nucleation and growth for a class of incompressible nonlinearly elastic materials, *Int. J. Solids Struct.*, **25**, 1239-1254.

GURSON A. L., 1977, Continuum theory of ductile rupture by void nucleation and growth — I. Yield criteria and flow rules for porous ductile media, *J. Engng. Materials Technol.*, **99**, 2-15.

HILL R., 1950, *The mathematical theory of plasticity*, Clarendon Press, Oxford.

HORGAN C. O. ABEYARATNE R., 1986, A bifurcation problem for a compressible nonlinearly elastic medium: growth of a microvoid, *J. Elasticity*, **16**, 189-200.

HOU H. -S., 1990, Work in progress, Ph. D. Thesis, Mass. Inst. of Technology.

HUANG Y., HUTCHINSON J. W., TVERGAARD V., 1989, *Cavitation instabilities in elastic-plastic solids*, Division of Appl. Sci., Harvard University, MECH-153.

HUTCHINSON J. W., 1973, Finite strain analysis of elastic-plastic solids and structures, in Numerical Solution of Nonlinear Structural Problems, R. F. HARTUNG ed., **17**, *ASME*, New York.

HUTCHINSON J. W., NEALE K. W., 1982, *Finite Elasticity*, D. E. CARLSON, R. T. SHIELD Eds., Nijhoff, Hague, 237-248.

MCCLINTOCK F. A., 1968, A criterion for ductile fracture by growth of holes, *J. Appl. Mech.*, **35**, 363-371.

MCMEEKING R. M., 1977, Finite deformation analysis of crack tip opening in elastic-plastic materials and implications for fracture, *J. Mech. Phys. Solids*, **25**, 357-381.

RICE J. R., TRACEY D. M., 1969, On the ductile enlargement of voids in triaxial stress fields, *J. Mech. Phys. Solids*, **17**, 201-217.

TVERGAARD V., 1982, On localization in ductile materials containing spherical voids, *Int. J. Fract.*, **18**, 237-252.

TVERGAARD V., 1990, Material failure by void growth to coalescence, *Adv. Appl. Mech.*, **27**, J. W. HUTCHINSON and T. Y. WU Eds., Academic Press, 83-151.

(Manuscript received September 20, 1990,
revised April 17, 1991;
accepted April 25, 1991.)